KINEMATICS OF IDEAL STRING VIBRATION AGAINST A RIGID OBSTACLE

Dmitri Kartofelev

Department of Cybernetics, School of Science,
Tallinn University of Technology,
Tallinn, Estonia
dima@ioc.ee

ABSTRACT

This paper presents a kinematic time-stepping modeling approach of the ideal string vibration against a rigid obstacle. The problem is solved in a single vibration polarisation setting, where the string's displacement is unilaterally constrained. The proposed numerically accurate approach is based on the d'Alembert formula. It is shown that in the presence of the obstacle the lossless string vibrates in two distinct vibration regimes. In the beginning of the nonlinear kinematic interaction between the vibrating string and the obstacle the string motion is *aperiodic* with constantly evolving spectrum. The duration of the aperiodic regime depends on the obstacle proximity, position, and geometry. During the aperiodic regime the fractional subharmonics related to the obstacle position may be generated. After relatively short-lasting aperiodic vibration the string vibration settles in the *periodic* regime. The main general effect of the obstacle on the string vibration manifests in the widening of the vibration spectra caused by transfer of fundamental mode energy to upper modes. The results presented in this paper can expand our understanding of timbre evolution of numerous stringed instruments, such as, the guitar, bray harp, tambura, veena, sitar, etc. The possible applications include, e.g., real-time sound synthesis of these instruments.

1. INTRODUCTION

Interaction and collision of a vibrating string with spatially distributed obstacles, such as fretboard or bridge, plays a significant role in the mechanics of numerous stringed musical instruments. One elegant example is the Medieval and Renaissance bray harp which has small bray-pins which provide a metal surface for the vibrating string to impact, increasing the upper partial content in the tone and providing a means for the harp to be audible in larger spaces and in ensemble with other instruments [1]. It is evident that for realistic physics-informed modeling of this instrument such nonlinearity inducing interactions need to be properly examined and understood.

The string–obstacle interaction modeling is a long-standing problem in musical acoustics. In the early twentieth century, Raman was first to study the problem and identify the veena bridge as the main reason for distinctive sounding of the tambura and veena. He noted that all string frequencies in these instruments are excited irrespective of the location of the excitation thereby violating the Young-Helmholtz law which states that the vibrations of a string do not contain the natural modes which have a node at the point of excitation. He notes that this is caused by the geometry of the bridge but did not explain the reason behind the inapplicability of the Young-Helmholtz law [2]. Since then, much effort has been devoted to modeling the collision dynamics of a vibrating string with various obstacles or boundary barriers. Over the years many authors have solved this problem using different approaches. The problem was considered by Schatzman [3] and Cabannes [4], who used the method of characteristics and assumed that the string does not lose energy when it hits an obstacle. Burridge *et al.* [5] assumed an inelastic constraint where the string is losing kinetic energy during contact. Ducceschi *et al.* [6], Krishnaswamy and Smith [7], Han and Grosenbaugh [8], Bilbao *et al.* [9], Bilbao [10], Chatziioannou and Walstijn [11], and Taguti [12] used a finite difference method to study the string interaction with the obstacle. Issanchou *et al.* [13], van Walstijn and Bridges [14], and van Walstijn *et al.* [15] used a modal analysis approach. Vyasarayani *et al.* [1], Mandal and Wahi [16], and Singh and Wahi [17] described the movement of the sitar string with partial differential equations or sets of partial differential equations. Rank and Kubin [18], Evangelista and Eckerholm [19], and Siddiq [20] used a waveguide modelling approach to study the plucked string vibration with nonlinear limitation effects.

This paper proposes an idealised approach for modeling the nonlinear string–obstacle interaction. We consider lossless ideal string vibration and assume that the obstacle is absolutely rigid. The interaction between the vibrating string and the obstacle is modeled in terms of kinematics, i.e., we study the string motion without considering its mass nor the possible inertial and reactional forces acting between the string and the obstacle during the collisions. The heuristics of our approach is directly determined by the d'Alembert formula (travelling wave solution). The results presented here are a continuation of the work published in [21].

The organisation of the paper is as follows. In Sec. 2, the string vibration modeling is explained. In Sec. 3 the problem description and the kinematic numerical model of string–obstacle interaction is presented and explained. Section 4 presents the results and analysis of three case studies, where the effects of the obstacle geometry, proximity, and position are considered. In Sec. 5 the presented results and the accuracy and efficiency of the numerical model are briefly commented on. Section 6 presents the main results and conclusions.

2. MODELING STRING VIBRATION

Let us consider the vibration of lossless ideal string in a single vibration polarisation setting. The one-dimensional equation of motion, called the wave equation, is in the following form:

$$\frac{\partial^2 u}{\partial t^2} = c^2 \frac{\partial^2 u}{\partial x^2}, \tag{1}$$

where $u(x,t)$ is the transverse displacement of the string, $c = \sqrt{T/\mu}$ is the speed of the waves travelling on the string, where T is the tension and μ is the linear mass density of the string, having the dimension [kg/m]. In the context of a real string Eq. (1)

can be used as an approximation of thin homogeneous elastic (and lossless) string vibration under a small amplitude restriction. In this case wave speed $c = \sqrt{T/(\rho A_\circ)}$, where ρ is the volumetric density, $A_\circ = \pi r^2$ is the cross-section area of a cylindrical string, and T is the tension. Equation (1) is studied, here, in a normalised and dimensionless form for increased clarity. We normalise the fundamental frequency f_0 by setting $c = 1$ and by introducing the following dimensionless variables:

$$t = \frac{\mathcal{T}}{P}, \quad x = \frac{X}{\lambda}, \quad u = \frac{U}{\lambda}, \tag{2}$$

where P is the fundamental period and λ is the corresponding wavelength. The dimensional quantities $\mathcal{T}$, X, and U are the time, space, and string displacement, respectively. Additionally, the speaking length L of the string is chosen to be a half of the wavelength, i.e., $L = 1/2$ [d. u.] (dimensionless units). This ensures that the fundamental frequency $f_0 = 1$ because for Eq. (1) it holds that

$$f_0 = \frac{c}{2L} = \frac{c}{\lambda}. \tag{3}$$

In order to further simplify the frequency domain analysis presented in Sec. 4 the following initial condition is selected: at $t = 0$ the string is freely released and the initial displacement is selected to be equal to the shape of the fundamental mode

$$u_0(x) = u(x, 0) = A \sin 2\pi x, \quad x \in [0, L], \tag{4}$$

$$\frac{\partial}{\partial t} u(x, 0) = 0, \quad x \in [0, L], \tag{5}$$

where $A = 1$ is the amplitude. This selection results in a sinusoidal (standing wave) vibration of all string points with fundamental frequency $f_0 = 1$ determined by the normalised Eq. (1). Figure 1 shows the initial condition (4).

It is well known that the Eq. 1 has an analytical solution known as the d'Alembert formula. For infinite string (ignoring boundary conditions for now) and for initial conditions (4), (5) the solution takes the following form:

$$u(x, t) = \frac{1}{2} \left(u_0(x - ct) + u_0(x + ct) \right). \tag{6}$$

This solution represents a superposition of two travelling waves: $u_0(x-ct)/2$ moving to the right (positive direction of the x-axis), and $u_0(x+ct)/2$ moving to the left. The function $u_0/2$ describing the shape of these waves stays constant with respect to x-axis, as they are translated in opposite directions at speed $c = 1$.

In the general case and under our assumptions a wave on any arbitrary segment of the string can be understood as a sum of two travelling waves that do not need to be equal. This means that one can write

$$u(x, t) = r(x - ct) + l(x + ct), \tag{7}$$

where $r(x - ct)$ is the travelling wave moving to the right and $l(x + ct)$ is the travelling wave moving to the left. Conveniently, one-dimensional advection equations

$$\frac{\partial r}{\partial t} + c \frac{\partial r}{\partial x} = 0, \tag{8}$$

$$\frac{\partial l}{\partial t} - c \frac{\partial l}{\partial x} = 0, \tag{9}$$

have similar general solutions. The travelling wave $r(x-ct)$, on its own, is also a solution to Eq. (8) and the travelling wave $l(x + ct)$ is a solution to Eq. (9). This result is not surprising because Eq. (1) can be factored into

$$\left[\frac{\partial}{\partial t} - c \frac{\partial}{\partial x} \right] \left[\frac{\partial}{\partial t} + c \frac{\partial}{\partial x} \right] u = 0. \tag{10}$$

Advection Eqs (8) and (9) are used below to numerically model the propagation of travelling waves. The finite difference method is used to approximate the solutions of these equations.

We discretise xt-plane into $n \times m$ discrete samples using a grid with equal step sizes in x and t directions. We discretise the x-axis with grid spacing $\Delta x = L/n$ and the t-axis with grid spacing $\Delta t = \Delta x = t_{\text{max}}/m$, where $m = 2n$. We let $x_i = i\Delta x$, where $0 \leq i \leq n$ and $t^j = j\Delta t$, where $0 \leq j \leq m$. From here it follows that $u_i^j = u(x_i, t^j)$, $r_i^j = r(x_i, t^j)$, and $l_i^j = l(x_i, t^j)$. A combination of step forward finite difference (FD) approximations of first order derivatives

$$\frac{\partial u}{\partial t} \approx \frac{u_i^{j+1} - u_i^j}{\Delta t}, \quad \frac{\partial u}{\partial x} \approx \frac{u_{i+1}^j - u_i^j}{\Delta x}, \tag{11}$$

and step backwards FD approximations

$$\frac{\partial u}{\partial t} \approx \frac{u_i^j - u_i^{j-1}}{\Delta t}, \quad \frac{\partial u}{\partial x} \approx \frac{u_i^j - u_{i-1}^j}{\Delta x}, \tag{12}$$

are used to approximate Eqs (8) and (9). Resulting FD approximations are in the following form:

$$r_i^{j+1} - r_i^j + c \frac{\Delta t}{\Delta x} (r_i^j - r_{i-1}^j) = 0, \tag{13}$$

$$l_i^{j+1} - l_i^j - c \frac{\Delta t}{\Delta x} (l_{i+1}^j - l_i^j) = 0. \tag{14}$$

Because $c = 1$ and $\Delta x = \Delta t$, in our case, the Courant number $c\Delta t/\Delta x = 1$ and the above expressions are simplified

$$r_i^{j+1} = r_{i-1}^j, \tag{15}$$

$$l_i^{j+1} = l_{i+1}^j. \tag{16}$$

By applying these rules for all grid points i and j one gets a simple translation of numerical values r_i^j and l_i^j propagating in opposite directions with respect to the x-axis (i-axis). This result agrees with the d'Alembert formula (7) and can be understood as a digital waveguide based on travelling wave decomposition and use of delay lines. The equivalence between FD approximation used here and digital waveguide modeling is shown in [22].

So far we have not addressed the boundary conditions of Eq. (1). We assume that the string is fixed at both ends. The following boundary conditions apply:

$$u(0, t) = u(L, t) = 0, \quad t \in [0, t_{\text{max}}], \tag{17}$$

where $t_{\text{max}} = 10P$ is the maximum integration time (size of the temporal domain). By applying boundary conditions (17) to the general solution (7) of the initial equation one finds for $x = 0$ the reflected travelling wave in the following form:

$$u(0, t) = r(-ct) + l(ct) = 0 \Rightarrow r(-ct) = -l(ct), \tag{18}$$

and similarly for $x = L$:

$$u(L, t) = r(L - ct) + l(L + ct) = 0 \Rightarrow \\ \Rightarrow l(L + ct) = -r(L - ct). \tag{19}$$

These results are discretised according to the FD discretisation scheme discussed above. The travelling wave (18) reflected from the left boundary at $x = 0$ is thus

$$r_0^j = -l_0^j, \quad j \in [0, m], \tag{20}$$

and the travelling wave (19) reflected from the right boundary at $x = L$ is

$$l_n^j = -r_n^j, \quad j \in [0, m]. \tag{21}$$

In order to obtain the resulting string displacement u_i^j, for the selected initial and boundary conditions, a superposition of travelling waves (15), (16), (20), and (21) is found in accordance with general solution (7)

$$u_i^j = r_i^j + l_i^j, \quad \{i, j\} \in [0, n] \times [0, m]. \tag{22}$$

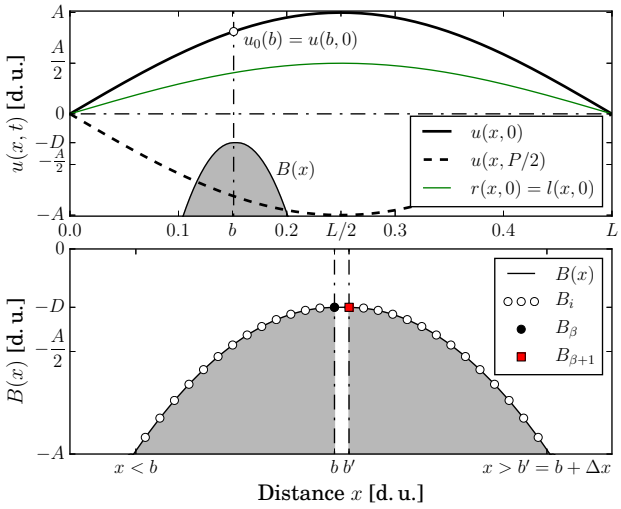

Figure 1: *Top: Schematic of the problem studied. The initial condition (4) and the corresponding travelling waves are presented. The obstacle is shown with the grey formation at $x = b$. The resting position of the string is shown with the horizontal dash-dotted line. Bottom: The cross-section profile $B(x)$ of the rigid parabolic obstacle and its discrete samples B_i, where $B_\beta = B_{\beta+1} = -D$.*

3. STRING–OBSTACLE INTERACTION KINEMATICS

Let us consider a smooth and absolutely rigid impenetrable obstacle. The obstacle is placed near the vibrating string so that it is able to obscure string's displacement $u(x, t)$. We select an obstacle with parabolic cross-section profile

$$B(x) = -\left[\frac{(x-b)^2}{2R} + D\right], \tag{23}$$

where $x = b$ is the position of the obstacle along the string, D is the vertical proximity of the obstacle to the string at its rest position, and R is the curvature radius of parabola at its apex. The function $B(x)$ is discretised according to the FD discretisation scheme presented in the previous Section. We let $B_i = B(x_i)$. Figure 1 shows the schematic drawing of the problem studied, the cross-section profile function $B(x)$ of the obstacle, and its discretised samples B_i.

The kinematic modeling of the string–obstacle interaction is a twofold problem. First, one needs to consider travelling wave $r(x - ct)$ approaching the obstacle form the left side. Second, one considers the travelling wave $l(x + ct)$ approaching the obstacle from the right side.

3.1. Reflection of travelling wave $r(x - ct)$

The heuristics of the following approach is strictly determined by the d'Alembert formula (6) or (7). Any change in string displacement $u(x, t)$ imposed by the obstacle must involve both travelling waves. The reflection of the travelling wave $r(x-ct)$ approaching the obstacle from the left is determined by a change in the travelling wave $l(x + ct)$. We assume that the travelling wave $l(x + ct)$ resulting from the interaction first appears, or already existing one is modified, only at the point $x = x^* \leq b$, where the amplitude of string displacement $u(x^*, t) < B(x^*)$, i.e., the string attempts to penetrate the obstacle. The position of this point x^* is determined by the obstacle profile geometry $B(x)$. Because, the obstacle is in fact impenetrable we must have $u(x^*, t) = B(x^*)$ at the moment of collision. This condition determines the shape of a *reflected* travelling wave

$$\hat{l}(x^*, t) = B(x^*) - u(x^*, t). \tag{24}$$

Once one has determined the shape of the *reflected* travelling wave (24) for given time moment. It is used inside the same time moment as a travelling wave $l(x+ct)$ or to modify the already existing travelling wave moving to the left in the following manner:

$$l(x^*, t) = l(x^*, t) + \hat{l}(x^*, t). \tag{25}$$

The above modification of the travelling wave $l(x+ct)$ simply ensures that the resulting string displacement $u(x^*, t) = r(x^*, t) + l(x^*, t)$ does not geometrically penetrate the obstacle during the collision.

In determining the points x^* one does not need to consider points $x > b$. In the absence of any waves approaching from the right and for $x^* = b$ the string displacement $u(b, t) = -D$ (caused by the reflection process explained in the next Subsection). This means that the string displacement $u(x, t)$ becomes truncated and equal to the maximum value of the obstacle as the propagating wave passes over its apex. This phenomenon is shown in Fig. 2 in the case of a short wavelength bell-shaped pulse reflecting from the obstacle during the first period of string vibration. Because the obstacle profile is an inverted parabola with its maximum at $x = b$ then for $x > b$ it holds that $u(x, t) > B(x) \Rightarrow x \neq x^*$.

Numerical implementation of the procedure is straightforward. We let $x_\beta = \beta\Delta x = b$ (see Fig. 1) and $x_{i*} = i^*\Delta x = x^*$. Using this notation the *reflected* travelling wave (24) takes the following form:

$$\hat{l}_{i*}^j = B_{i*} - u_{i*}^j, \quad i \in [0, \beta]. \tag{26}$$

The resulting reflection and consequent string shape according to (22) and (25) for grid points i^* becomes

$$u_{i*}^j = r_{i*}^j + l_{i*}^j, \quad i \in [0, \beta], \tag{27}$$

where

$$l_{i*}^j = l_{i*}^j + \hat{l}_{i*}^j, \quad i \in [0, \beta]. \tag{28}$$

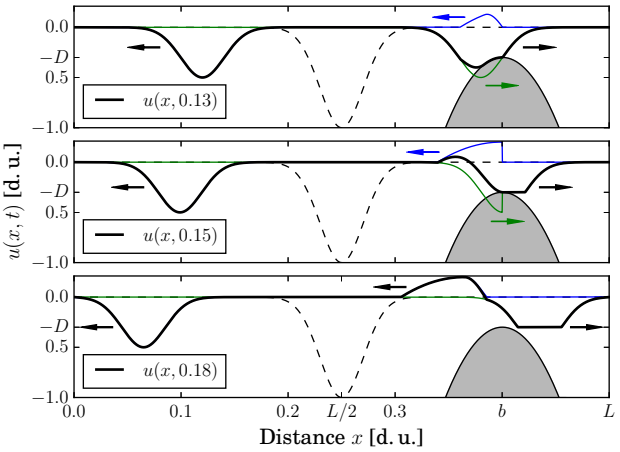

Figure 2: *Reflection of travelling wave $r(x-ct)$, shown with the thin green line, from the obstacle that is shown with the grey formation. The reflected travelling wave $\hat{l}(x+ct)$ is shown with the thin blue line. Arrows indicate the directions of wave propagation. Bell-shaped initial condition is shown with the dashed line.*

3.2. Reflection of travelling wave $l(x+ct)$

The determination of the reflection of travelling wave $l(x+ct)$ approaching the obstacle from the right side is similar to the previous case. In fact, it is a mirror image of that problem with symmetry axis at $x=b$. However, there is a slight difference in the region where it is necessary to evaluate and determine the points $x=x^*$. This difference stems from the selection and mathematical definition of the obstacle cross-section profile (23), namely, the function $B(x)$, being a unimodal function, has one maximum $\max B(x) = -D$ at $x=b$. The problem arises from the fact that one has already evaluated this point inside the same time moment t and used it to calculate the reflection of travelling wave $r(x-ct)$. By using this point again one would introduce a discontinuity in the string displacement $u(x,t)$. In principle it is not possible to use some other closely located neighbouring point, e.g., $x=b'=b+\Delta x$ (see Fig. 1). This selection, too, would introduce a small discontinuity due to $B(b)\neq B(b')$, and more importantly, in a continuous domain of real numbers there is no such thing as a neighbouring number (point) because one can always find infinitely many numbers between any two real numbers. One way of resolving this problem is to slightly modify the discretised approximation of the obstacle profile B_i as shown in Fig. 1. One simply squeezes in a second maximum point $B_{\beta+1}=-D$ after grid point $i=\beta$ corresponding to $x_\beta=\beta\Delta x=b$. Because $\Delta x \ll 1$ the overall change introduced in B_i compared to $B(x)$ remains negligibly small.

Let us formalised the result. Similarly to the previous case only at the points $x=x^*\geq b'\simeq b$, where by definition and during the collision $u(x^*,t)<B(x^*)$, a reflected travelling wave moving to the right is introduced or existing one is modified

$$r(x^*,t)=r(x^*,t)+\hat{r}(x^*,t), \tag{29}$$

where

$$\hat{r}(x^*,t)=B(x^*)-u(x^*,t). \tag{30}$$

Numerical implementation, using the notation proposed in the previous Subsection, takes the following form: the resulting reflection and consequent string shape according to (22), (29), and (30) for grid points i^* is

$$u^j_{i*}=r^j_{i*}+l^j_{i*}, \quad i\in(\beta,n], \tag{31}$$

where

$$r^j_{i*}=r^j_{i*}+\hat{r}^j_{i*} \text{ and } \hat{r}^j_{i*}=B_{i*}-u^j_{i*}, \text{ if } i\in(\beta,n], \tag{32}$$

4. RESULTS

Next, three case studies are considered. The effects of varying the values of the obstacle radius R (Sec. 4.1), obstacle proximity D (Sec. 4.2), and position b (Sec. 4.3), while keeping other system parameters constant, on the string vibration are analysed. Table 1 displays the values of parameters used in the case studies.

Table 1: *Values of the parameters used in the case studies. The parameter that is being varied is indicated with the grey background.*

Sec.	Radius R [d. u.]	Proximity D [d. u.]	Position b [d. u.]
4.1	$1\cdot10^{-5}$ $6\cdot10^{-3}$	$0.5\,u_0(b)=0.29$	$L/5=1/10$
4.2	$3\cdot10^{-3}$	$0.3\,u_0(b)=0.26$ $0.1\,u_0(b)=0.09$	$L/3=1/6$
4.3	$4\cdot10^{-3}$	$0.35\,u_0(b)=0.30$ $0.35\,u_0(b)=0.21$	$L/3=1/6$ $L/5=1/10$

The proximity D of the obstacle to the string at its rest position is expressed in terms of the initial condition (4). Namely, the string displacement $u_0(x)=u(x,0)$ at obstacle location $x=b$ (see Fig. 1). This is done in order to make the results comparable to each other. All frequency domain result are calculated using time series of the string displacement $u(x,t)$ recorded at $x=x_r=0.47L=0.235$. This point is close to a node at $x=L/2$ shared by all even numbered modes (harmonics or overtones). The reader must keep in mind that this selection results in relatively small amplitude values of even numbered modes in the spectra presented below. On the other hand, this selection ensures that the amplitude of fundamental mode is nearly unity for the linear case where the obstacle is absent. This, in turn, will aid in drawing the conclusions. The spectrograms of power spectra, amplitude spectra, spectral centroid $\langle f\rangle$, and instantaneous spectral centroid $\langle f'\rangle(t)$ are calculated using fast Fourier transform algorithm which is based on the Fourier transform. In calculating spectrograms a sliding window approach, in combination with the Hanning window function, is used. Here, window size $t=3P$ and window overlap value is 50% of the window size. Instantaneous spectral centroid $\langle f'\rangle(t)$ is also calculated using the windowing approach with window size $t=P$ and with window overlap value 70% of the window size. Video animations of the string vibrations for all case studies presented below can be downloaded at the accompanying web-page of this paper[1]. The web-page also includes an additional example of a symmetric case where the obstacle is positioned at the midpoint of the string at $b=L/2$.

4.1. Effect of the obstacle radius

Figure 3 shows the influence of varying the value of obstacle radius R on the string shape $u(x,t)$ for the duration of the first period

[1] http://www.ioc.ee/~dima/dafx17.html

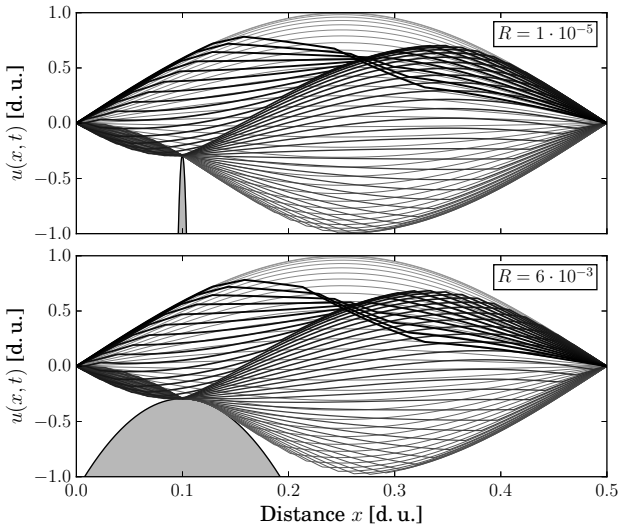

Figure 3: *Stroboscopic plot of the string displacement during the first period of vibration where $t \in [0, P]$. Showing 68 time steps. The thickness of the lines is proportional to the direction of time flow. The obstacles with radius $R = 1 \cdot 10^{-5}$ (top) and $R = 6 \cdot 10^{-3}$ (bottom) are positioned at $b = L/5$ and $D = u_0(b)/2$.*

only. The results of frequency domain analysis of the resulting vibration are shown in Fig. 4. Visual inspection of the time series $u(x_r, t)$ reveals that the string vibrates in two distinct vibration regimes (generally true for all presented case studies). The initial strong influence of the obstacle is manifested in the constantly evolving spectrum that prolongs for $t = t_p$. We call this regime the *aperiodic* regime. After $t = t_p$ the string vibration settles in the *periodic* regime, where the spectrum remains constant. Time moment t_p corresponds to the latest time instance where point x^* is determined.

During the aperiodic regime the value of instantaneous spectral centroid grows with the time (generally true for all presented case studies) resulting in the value of spectral centroid that is one octave (two times) greater compared to the linear case where the obstacle is absent (in linear case $\langle f' \rangle(\infty) = \langle f \rangle = f_0 = 1$). The growth of the value of spectral centroid is driven by nonlinear widening of the spectrum caused by transfer of the fundamental mode energy to higher modes. For both presented cases and according to the amplitude spectra, shown in Fig. 4, approximately 65% of initial fundamental mode amplitude $A = 1$ is redistributed to and between the higher modes. Mutual comparison of the cases shows that the case with larger radius R results in approximately one-third shorter-lasting aperiodic regime and slightly higher value of spectral centroid. A relatively large change in the obstacle radius R has a moderate effect (compared to the other case studies) on the final string vibration—at least for the given parameter values. This is best seen in roughly equal amplitude spectra.

4.2. Effect of the obstacle proximity

Figure 5 shows the influence of varying the value of the obstacle proximity D on the string shape $u(x, t)$ for the duration of the first period only. The results of frequency domain analysis of the vibration are shown in Fig. 6. Inspection of the aperiodic regime

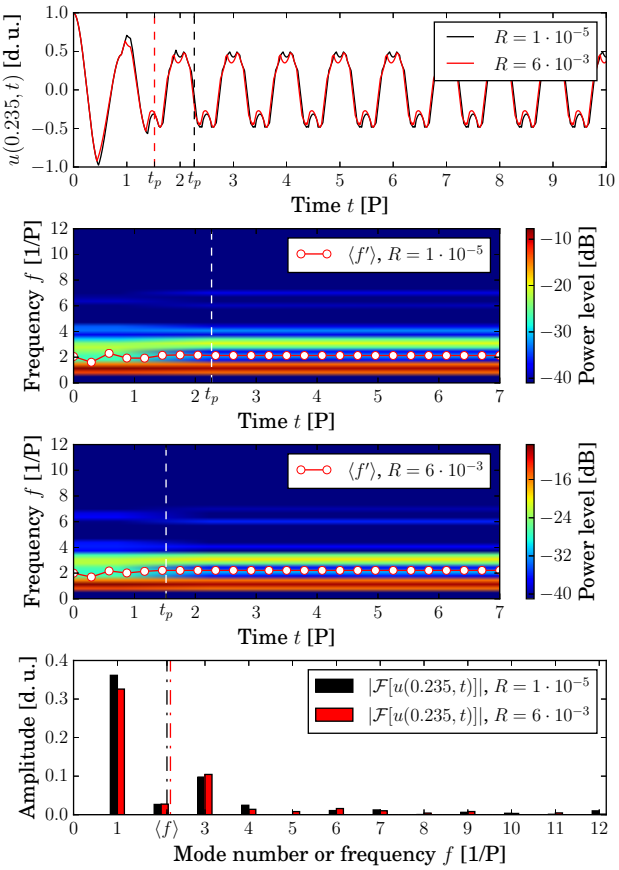

Figure 4: *Top: Time series $u(x_r, t)$ shown for two values of the obstacle radius R. Onset time t_p of the periodic regime shown with the colour-coded dashed line. Middle: Power spectrograms. Instantaneous spectral centroid $\langle f' \rangle$ is shown with the solid red line marked with bullets. Onset time t_p of the periodic regime is shown with the dashed white line. Bottom: Amplitude spectra in the periodic regimes where $t \in [\lceil t_p \rceil, t_{max}]$. Spectral centroid $\langle f \rangle$ is shown with the colour-coded dash-dotted line.*

of both cases shows that a short-lasting large amplitude fractional subharmonic at $f = 1.5$ is generated. This partial does not survive the aperiodic regime. Based on the relationship (3) one can conclude that this frequency is related to the fact that the obstacle is promoting a node at $b = L/3$ by effectively dividing the string into two vibrating segments with lengths $L/3$ and $2L/3$.

Comparison of the periodic regime vibration to the linear case shows that the resulting value of spectral centroid is increased by almost four to five octaves depending on the case. As in the previous case study the string–obstacle interaction has widened the spectrum at the expense of the fundamental mode. The resulting fundamental mode amplitude, for both cases, is approximately 0.02. This means that during the aperiodic regime more than 97% of initial mode amplitude $A = 1$ is redistributed to higher modes. The greatest relative and absolute change in mode amplitude, caused by the reduction of the distance D between the string and the obstacle, is seen for the third and tenth modes. The amplitude of third mode is grown two times from approximately 0.02 to approximately 0.04. The amplification of the third mode is

related to the obstacle position b discussed above. Mutual comparison of the presented cases shows that the case where the obstacle is closer to the string results in approximately three times longer-lasting aperiodic regime and in the value of spectral centroid that is greater by an octave.

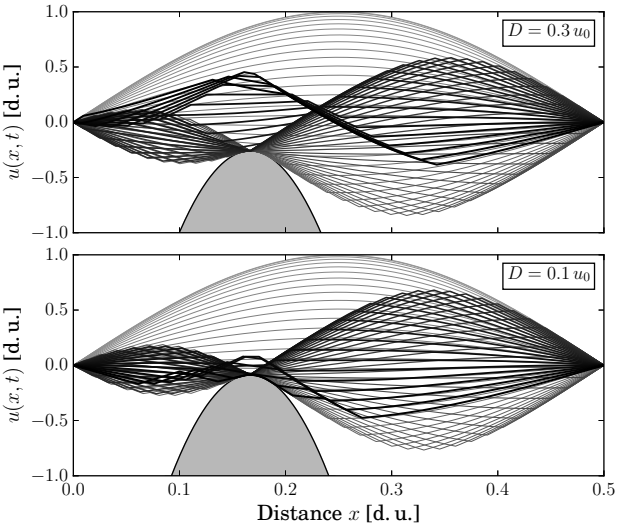

Figure 5: *Stroboscopic plot of the string displacement during the first period of vibration where $t \in [0, P]$. Showing 68 time steps. The thickness of the lines is proportional to the direction of time flow. The obstacle with radius $R = 3 \cdot 10^{-3}$ is positioned at $b = L/3$. The obstacle with proximity $D = 0.3\,u_0(b)$ (top) and $D = 0.1\,u_0(b)$ (bottom) are presented.*

4.3. Effect of the obstacle position along the string

Figure 7 shows the influence of varying the value of the obstacle position b on the string shape $u(x,t)$ for the duration of the first period only. The results of frequency domain analysis of the vibration are shown in Fig. 8. Inspection of the aperiodic regime shows, similarly to the previous case study, that short-lasting subharmonic at $f = 1.5$ and at $f = 1.25$ are generated for the cases where $b = L/3$ and $b = L/5$, respectively. The cause for these large amplitude partials is the same as discussed in the previous case study.

Comparison of the periodic regime to the linear case shows that the resulting value of spectral centroid has increased by approximately three octaves, in both cases. In contrast to the previous case study the inspection of the spectra in the periodic regime shows no significant amplification of third and fifth modes related to the obstacle positions b. In fact we see a significant reduction of the fifth mode as we move the obstacle closer to the string edge ($x = 0$). In addition to the nonlinearity, the absence of these modes may be explained by obstacle's ability (related to the profile geometry) to elongate the segments of travelling waves that kinematically reflect from it, see Fig. 2 [21]. If this is the case the obstacle is redistributing the energy of these modes to neighbouring lower modes. Also, the amplitudes of these expected modes may be masked by a process of constant and progressive trimming of the amplitudes of travelling waves during the aperiodic regime discussed and shown in Sec. 3.1 and Fig. 2, respectively. This result is to demonstrate that, when dealing with nonlinear systems,

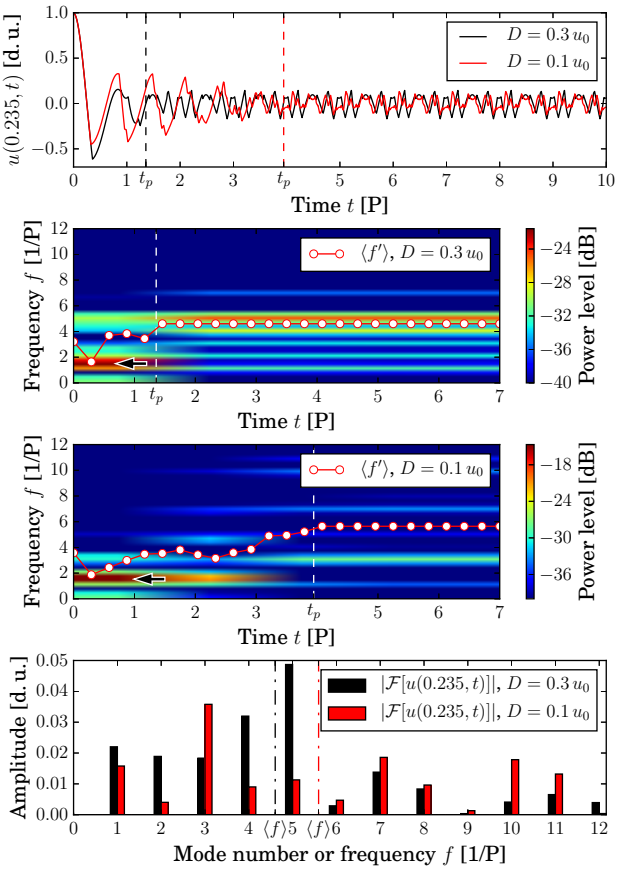

Figure 6: *Top: Time series $u(x_r, t)$ shown for two values of the obstacle proximity D. Onset time t_p of the periodic regime shown with the colour-coded dashed line. Middle: Power spectrograms. Instantaneous spectral centroid $\langle f' \rangle$ is shown with the solid red line marked with bullets. Onset time t_p of the periodic regime is shown with the dashed white line. Subharmonic at $f = 1.5$ is shown with the bold arrow. Bottom: Amplitude spectra in the periodic regime where $t \in [\lceil t_p \rceil, t_{max}]$. Spectral centroid $\langle f \rangle$ is shown with the colour-coded dash-dotted line.*

each problem needs to be studied on a case by case basis.

Mutual comparison of presented cases shows that the final value of spectral centroid differs by half of an octave. The case where the obstacle is positioned closer to the string edge results in approximately two times longer-lasting aperiodic regime. The resulting fundamental mode amplitude is approximately 0.05 for $b = L/3$ and 0.1 for $b = L/5$ meaning that during the aperiodic regime approximately 90 to 95% of initial mode amplitude $A = 1$ is redistributed between the higher modes.

5. DISCUSSION

The method of modeling the string–obstacle interaction presented in this paper is probably the most simplified and idealised approach that is still able to retain scientific relevance and provide a useful insight into more realistic problems. The idealised nature of the method guarantees numerical accuracy and allows for efficient and simple implementation. This fact cannot be ignored when dealing

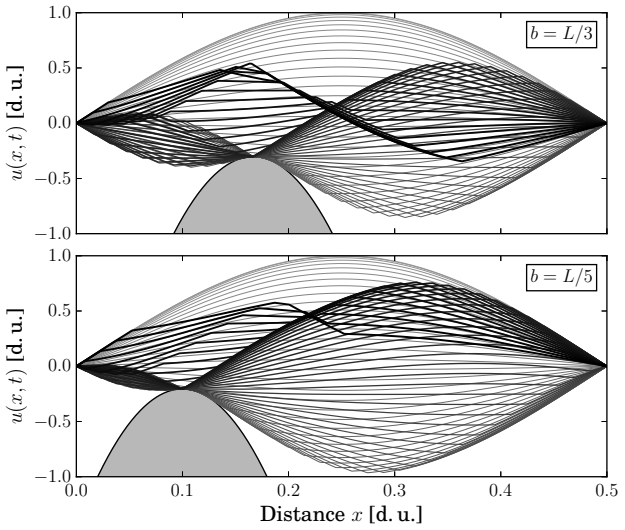

Figure 7: *Stroboscopic plot of the string displacement during the first period of vibration where $t \in [0, P]$. Showing 68 time steps. The thickness of the lines is proportional to the direction of time flow. The obstacle with radius $R = 4 \cdot 10^{-3}$ is positioned at $b = L/3$ (top) and $b = L/5$ (bottom), and in both cases $D = 0.35\, u_0(b)$.*

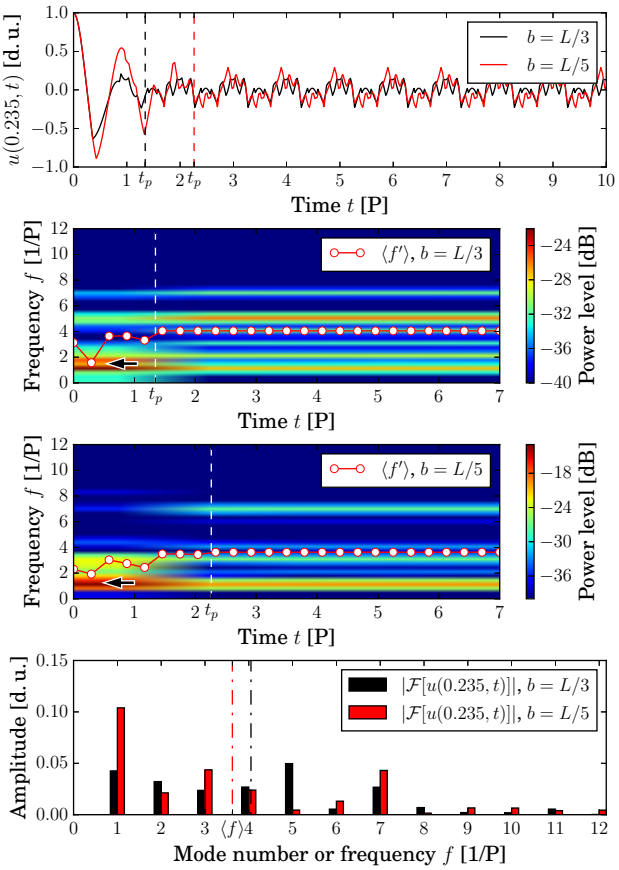

Figure 8: *Top: Time series $u(x_r, t)$ shown for two values of obstacle position b. Onset time t_p of the periodic regime shown with the colour-coded dashed line. Middle: Power spectrograms. Instantaneous spectral centroid $\langle f' \rangle$ is shown with the solid red line marked with bullets. Onset time t_p of the periodic regime shown with the dashed white line. Subharmonics at $f = 1.5$ and $f = 1.25$ are shown with the bold arrows. Bottom: Amplitude spectra in the periodic regime where $t \in [\lceil t_p \rceil, t_{max}]$. Spectral centroid $\langle f \rangle$ is shown with the colour-coded dash-dotted line.*

with nonlinear problems of this type. Physically more comprehensive and thus more realistic mathematical descriptions of string–obstacle collision problems often result in rather complicated nonlinear equations of motion or in systems of equations. Modeling of these problems then rely on numerical integration of these equations. This in itself can pose a great technical challenge and the obtained solutions may be contaminated by numerical dispersion and other accumulative round-off or approximation errors inherent in most iterative numerical methods. For example in [10, 14] the iterative solvers are avoided altogether when solving the problem of lossy stiff string vibration against an obstacle.

The numerical accuracy of the proposed approach is mainly a result of an adept FD discretisation of the problem domain (xt-plane), discussed in Sec. 2, which ensures that at no iteration step does the method rely on multiplication or division of rounded-off numerical values. This guarantees that the resulting numerical solution lacks any accumulative approximation errors and the round-off errors are minimal. Travelling waves are modeled as translations of numerical values along the iteration axes, according to (15) and (16). The string interaction with the obstacle is calculated, according to (24) and (30), using only subtraction or addition operations. In fact, assuming perfect arithmetics, i.e., assuming no round-off, one could predict the motion of a string, undergoing a kinematic string–obstacle interaction, for infinite number of iterations without losing any accuracy.

The proposed approach can be applied for estimating the effect that an obstacle with various cross-section profiles has on a string vibration. In principle the function $B(x)$ can be chosen arbitrarily as long as one remembers to modify its FD discretisation at maximum or local maxima (in the case of more general multimodal and/or discontinuous functions) as explained in Sec. 3.2. Additionally, the model can be use to study the effects of different initial and plucking conditions (including dynamic ones) on the string–obstacle system. It is reasonable to assume that proposed model can generate these results faster compared to more sophisticated models, which is often desired in real-time simulation applications. In connection with other methods of signal processing and sound synthesis the presented model can be used to synthesise timbres of stringed instruments that are equipped with nonlinearity inducing obstacles, such as, frets, bridges, and nuts.

6. CONCLUSIONS

In this paper the kinematics of ideal string vibration against an absolutely rigid obstacle was modeled using the approach based on the application of the d'Alembert formula as explained in Sec. 3. The presented numerical method is accurate and efficient lacking numerical dispersion caused by accumulative approximation errors. The effect of the obstacle proximity D on the string vibration and on the mean level of upper mode amplitudes was clearly evi-

dent and this was to confirm that the problem is nonlinear.

It was shown that the ideal lossless string interacting with the obstacle vibrates in two distinct vibration regimes. In the beginning of the kinematic interaction between the vibrating string and the obstacle the string motion is *aperiodic* with constantly evolving spectrum. After some time of aperiodic vibration the string vibration settles in the *periodic* regime where the string motion is repetitious in time. The duration of the aperiodic regime depends on the obstacle proximity D, position b, and geometry (curvature radius R). The comparison of the resulting spectra in the periodic regime with the linear case where the obstacle was missing showed that the general effect of the obstacle manifests in the widening of the spectrum caused by transfer of fundamental mode energy to upper modes. The analysis of the relatively short-lasting aperiodic regime showed that the obstacle position b may generate temporary fractional subharmonics related to the node point at $x = b$. In conclusion, the results presented in this paper can expand our understanding of timbre evolution of numerous stringed instruments, such as, the guitar, bray harp, tambura, veena, sitar, etc. The possible applications include, e.g., sound synthesis of these instruments.

7. ACKNOWLEDGMENTS

This research was supported by the Estonian Ministry of Education and Research, Project IUT33-24, and by Doctoral Studies and Internationalisation Programme DoRa Plus Action 1.1 (Archimedes Foundation, Estonia) through the ERDF. The author is grateful to the anonymous reviewers of this paper—their suggestions improved the manuscript greatly.

8. REFERENCES

[1] C. P. Vyasarayani, S. Birkett, and J. McPhee, "Modeling the dynamics of a vibrating string with a finite distributed unilateral constraint: Application to the sitar," *The Journal of the Acoustical Society of America*, vol. 125, no. 6, pp. 3673–3682, 2009.

[2] C. V. Raman, "On some Indian stringed instruments," *Proceedings of the Indian Association for the Cultivation of Science*, vol. 7, pp. 29–33, 1921.

[3] M. Schatzman, "A hyperbolic problem of second order unilateral constraints: the vibrating string with a concave obstacle," *Journal of Mathematical Analysis and Applications*, vol. 73, no. 1, pp. 138–191, 1980.

[4] H. Cabannes, "Presentation of software for movies of vibrating strings with obstacles," *Applied Mathematics Letters*, vol. 10, no. 5, pp. 79–84, 1997.

[5] R. Burridge, J. Kappraff, and C. Morshedi, "The sitar string, a vibrating string with a one-sided inelastic constraint," *SIAM Journal on Applied Mathematics*, vol. 42, no. 6, pp. 1231–1251, 1982.

[6] M. Ducceschi, S. Bilbao, and C. Desvages, "Modelling collisions of nonlinear strings against rigid barriers: Conservative finite difference schemes with application to sound synthesis," in *Proc. of 22nd International Congress on Acoustics (ICA 2016)*, Buenos Aires, Argentina, Sept. 5–9 2016, pp. 1–11.

[7] A. Krishnaswamy and J. O. Smith, "Methods for simulating string collisions with rigid spatial obstacles," in *Proc. of IEEE Workshop on Applications of Signal Processing to Audio and Acoustics*, New Paltz, NY, USA, 2003, pp. 233–236.

[8] S. M. Han and M. A. Grosenbaugh, "Non-linear free vibration of a cable against a straight obstacle," *Journal of Sound and Vibration*, vol. 237, pp. 337–361, 2004.

[9] S. Bilbao, A. Torin, and V. Chatziioannou, "Numerical modeling of collisions in musical instruments," *Acta Acustica United With Acustica*, vol. 101, no. 1, pp. 155–173, 2012.

[10] S. Bilbao, "Numerical modeling of string/barrier collisions," in *Proc. of International Symposium on Musical Acoustics (ISMA 2014)*, Le Mans, France, Jul. 7–12 2014, pp. 1–6.

[11] V. Chatziioannoua and M. van Walstijn, "Energy conserving schemes for the simulation of musical instrument contact dynamics," *Journal of Sound and Vibration*, vol. 339, pp. 262–279, March 2015.

[12] T. Taguti, "Dynamics of simple string subject to unilateral constraint: A model analysis of sawari mechanism," *Acoustical Science and Technology*, vol. 29, no. 3, pp. 203–214, 2008.

[13] C. Issanchou, S. Bilbao, J.-L. Le Carrou, C. Touzé, and O. Doaré, "A modal-based approach to the nonlinear vibration of strings against a unilateral obstacle: Simulations and experiments in the pointwise case," *Journal of Sound and Vibration*, vol. 393, pp. 229–251, April 2017.

[14] M. van Walstijn and J. Bridges, "Simulation of distributed contact in string instruments: a modal expansion approach," in *Proc. of 24th European Signal Processing Conference (EUSIPCO-2016)*, Budapest, Hungary, Aug. 29–Sept. 2 2016, pp. 1–5.

[15] M. van Walstijn, J. Bridges, and S. Mehes, "A real-time synthesis oriented tanpura model," in *Proc. of 19th International Conference on Digital Audio Effects (DAFx-16)*, Brno, Czech Republic, Sept. 5–9 2016, pp. 175–182.

[16] A. K. Mandal and P. Wahi, "Natural frequencies, modeshapes and modal interactions for strings vibrating against an obstacle: Relevance to sitar and veena," *Journal of Sound and Vibration*, vol. 338, pp. 42–59, March 2015.

[17] H. Singh and P. Wahi, "Non-planar vibrations of a string in the presence of a boundary obstacle," *Journal of Sound and Vibration*, vol. 389, pp. 326–349, February 2017.

[18] E. Rank and G. Kubin, "A waveguide model for slapbass synthesis," in *Proc. of IEEE International Conference on Acoustics, Speech, and Signal Processing*, Munich, Germany, 1997, pp. 443–446.

[19] G. Evangelista and F. Eckerholm, "Player–instrument interaction models for digital waveguide synthesis of guitar: touch and collisions," *IEEE Transactions on Audio, Speech, and Language Processing*, vol. 18, no. 4, pp. 822–832, 2010.

[20] S. Siddiq, "A physical model of the nonlinear sitar string," *Archives of Acoustics*, vol. 37, no. 1, pp. 73–79, 2012.

[21] D. Kartofelev, A. Stulov, H.-M. Lehtonen, and V. Välimäki, "Modeling a vibrating string terminated against a bridge with arbitrary geometry," in *Proc. of 4th Stockholm Music Acoustics Conference (SMAC 2013)*, Stockholm, Sweden, Jul. 30–Aug. 3 2013, pp. 626–632.

[22] J. O. Smith, *Physical Audio Signal Processing for Virtual Musical Instruments and Audio Effects*, W3K Publishing, 2010.